

Photoelectron spectroscopy of small antimony cluster anions: Sb^- , Sb_2^- , Sb_3^- , and Sb_4^-

Mark L. Polak, Gustav Gerber,^{a)} Joe Ho,^{b)} and W. C. Lineberger

Joint Institute for Laboratory Astrophysics, University of Colorado and National Institute of Standards and Technology, Boulder, Colorado 80309 and Department of Chemistry and Biochemistry, University of Colorado, Boulder, Colorado 80309

(Received 3 August 1992; accepted 8 September 1992)

We report the 351 nm photoelectron spectra of Sb^- , Sb_2^- , Sb_3^- , and Sb_4^- . The electron affinity of atomic Sb is measured to be 1.046(5) eV. The Sb_2^- photoelectron spectrum displays rich vibrational and electronic structure. Low-lying electronically excited states are observed for both the anion and the neutral. Several features in both the 351 and 364 nm photoelectron spectra of Sb_2^- cannot be explained as Franck–Condon processes, indicating that we are accessing autodetaching resonances of the negative ion at these wavelengths. The adiabatic electron affinity of Sb_2 is determined to be 1.282(8) eV. For the photoelectron spectra of Sb_3^- and Sb_4^- , the observed electronic structure is explained in terms of recently reported *ab initio* calculations. The adiabatic electron affinity of Sb_3 is estimated to be 1.85(3) eV, and an upper bound on the electron affinity of Sb_4 is reported, $\text{EA}(\text{Sb}_4) < 1.00(10)$ eV. The vertical detachment energies of Sb_3^- and Sb_4^- to the neutral ground states are determined to be 1.90(2) and 1.57(5) eV, respectively. We report photoelectron angular distributions for all the observed spectra, and find that the autodetaching resonance causes unusual angular distributions for Sb_2^- photodetachment. Finally, electron affinity trends for group V atoms, dimers, and small clusters are discussed in light of the present study.

I. INTRODUCTION

The structural and electronic properties of small metal clusters have generated considerable interest in recent years.¹ Not only do small metal clusters provide a basis for understanding the transition from molecular to bulk behavior in metals, but they also represent a unique class of chemical compounds which, despite much recent progress, remains largely uncharacterized. Negative ion photoelectron spectroscopy has proven to be an especially powerful technique for probing basic properties of small clusters. Recently, we have applied this technique to main group metals in studies of the group V clusters,² Bi_{2-4}^- , and of the group IV dimers,³ Sn_2^- , Pb_2^- , and SnPb^- . In general, the photoelectron spectra have displayed a complex yet understandable electronic structure, providing an overview of the low-lying electronic states of the corresponding neutral species. In the present paper, we report a similar study of another set of group V clusters, Sb_n^- ($n=1-4$).

Atomic antimony and small antimony clusters, mainly Sb_2 and Sb_4 , have been the subject of some spectroscopic investigation. The electronic structure of atomic Sb is well characterized.⁴ The electron affinity of Sb has been measured to be 1.07 ± 0.05 eV using photodetachment threshold spectroscopy.⁵

A comprehensive review of experimental and theoretical studies of the electronic structure of Sb_2 has been published by Balasubramanian.⁶ The spectroscopic investiga-

tions of interest for our study are those which have probed the low-lying electronic states accessible with our photoelectron spectrometer ($< 17\,000\text{ cm}^{-1}$ above the ground state of Sb_2). Of these, only the $X^1\Sigma_g^+(0_g^+)$ (Ref. 7) and the $A^3\Delta_u(1_u)$ (Ref. 8) states have been characterized by experiments. Balasubramanian and Li⁹ have performed high-level *ab initio* calculations on 44 electronic states below $44\,000\text{ cm}^{-1}$, including relativistic configuration-interaction (RCI) treatments for many of these states. These previous experimental and theoretical efforts will be discussed in relation to the photoelectron spectrum.

Antimony trimer has not been observed spectroscopically. Using matrix-isolation spectroscopy, Sontag and Weber¹⁰ tentatively assigned a resonance Raman feature to the trimer; however, in a subsequent study¹¹ the feature was reassigned to Sb_4 . Balasubramanian, Sumathi, and Dai¹² have performed quantum-chemical calculations on Sb_3 to estimate the energies of the five lowest electronic states corresponding to a triangular structure.

Antimony tetramer is the primary component of the antimony vapor¹³ and has been the subject of several matrix-isolation spectroscopic investigations. Sontag and Weber¹⁰ and Bondybey, Schwartz, and Griffiths¹⁴ have used Raman spectroscopy to determine fundamental vibrational frequencies; the results were consistent with a tetrahedral geometry. Recently, Zhang and Balasubramanian¹⁵ have performed high-level quantum-chemical calculations on the lowest six electronic states of tetrahedral Sb_4 .

Wang and co-workers have reported the HeI (584 Å) photoelectron spectra of both antimony dimer¹⁶ and tetramer,¹⁷ probing the electronic structures of the respective cations. The tetramer photoelectron spectrum provides some interesting comparisons to our Sb_4^- spectrum. The

^{a)}Joint Institute for Laboratory Astrophysics Visiting Fellow. Permanent address: Fakultät für Physik, Universität Freiburg, W-7800 Freiburg, Federal Republic of Germany.

^{b)}Current address: Chemistry Division, Argonne National Laboratory, Argonne, Illinois 60439-3473.

thermochemistry of small antimony clusters has been of some interest as well. Kordis and Gingerich¹⁸ have used Knudsen effusion mass spectrometry to determine heats of atomization for Sb_{2-4} . Combining these values with electron affinities leads to the determination of thermodynamic stabilities for the respective anions.

In the present study we report the 351 nm photoelectron spectra of Sb_{1-4}^- . To our knowledge, there have been no previous spectroscopic studies of the negative ions, except for Sb^- .⁵ First, we present a brief description of the experimental methods. Next, the individual photoelectron spectra are presented and analyzed, and the results are compared to previous spectroscopy and quantum-chemical calculations. Then the photoelectron angular distributions measured for all four species are presented and discussed. Finally, the trends observed for the electron affinities of small group V clusters are discussed.

II. EXPERIMENT

The cold cathode discharge metal cluster source¹⁹ and the photoelectron spectrometer²⁰ have been described previously in detail; only the basic features are summarized here. Ions are formed in an antimony cathode discharge source. The cathode consists of an approximately 8 cm long piece of a 1 cm diameter antimony rod (Aesar, 99.9% purity), and is maintained at -2 to -4 kV with respect to ground. In this manner, a discharge is struck between the cathode and the chamber walls. The primary carrier gas is helium [500 mTorr, 4 standard liters per minute (SLPM)], seeded with approximately 10% argon to promote sputtering. The ions are allowed to equilibrate with the carrier gas in a 0.25 m long flow tube, at the end of which the negative ions are extracted through a 0.5 mm pinhole into a differentially pumped region. Typical ion currents, measured at a Faraday cup at the end of the beamline, are 5 pA of Sb^- , 45 pA of Sb_2^- , 125 pA of Sb_3^- , and 450 pA of Sb_4^- .

Following extraction, the ions are mass selected by a Wien filter, and the mass-selected ions are crossed by 351 or 364 nm laser light. Electrons ejected perpendicular to the laser-beam-ion-beam plane are collected and energy analyzed in a hemispherical analyzer with 8–10 meV resolution. The absolute energy scale is calibrated against the precisely known electron affinity of oxygen,²¹ and the relative energy scale is calibrated against the energy-level spacings⁴ of tungsten and antimony atoms, as measured in the photoelectron spectra of the atomic anions. The absolute position of a well-resolved peak can be measured to an accuracy of ± 5 meV. The photoelectron spectra are expressed in terms of electron kinetic energy (eKE) or electron binding energy (eBE = $h\nu - \text{eKE}$). The electron binding energy of a transition does not change with photon energy.

Because the electron collection angle is fixed, the angular dependence of the photodetachment cross section can be studied by rotating the laser polarization with a half-wave plate. In the electric dipole approximation, the angular dependence of a photodetachment cross section is given by²²

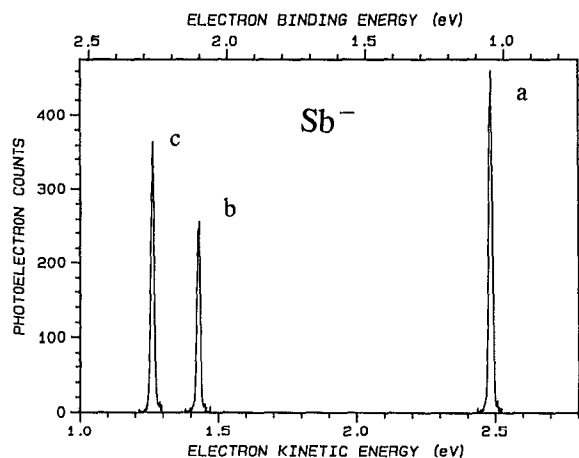


FIG. 1. The 351 nm photoelectron spectrum of Sb^- . From the position of peak a, we determine an electron affinity for atomic antimony of 1.046(5) eV.

$$d\sigma/d\Omega = (\sigma_0/4\pi) [1 + (\beta/2)(3 \cos^2 \theta - 1)], \quad (1)$$

where θ is the angle between the laser polarization vector and the direction of electron ejection, and β is the asymmetry parameter ($-1 \leq \beta \leq 2$). Generally, the laser polarization is set at the “magic angle” (54.7° where $3 \cos^2 \theta - 1 = 0$) such that the spectral intensities are proportional to the total photodetachment cross section. In order to measure β for each transition the photoelectron spectra are measured at $\theta = 0^\circ$ and $\theta = 90^\circ$. To determine β accurately for individual peaks, the angular dependence of the largest peaks in the spectra are measured in 10° intervals, and the observed intensities are least-squares fit to Eq. (1). These values of β can then be used to scale the $\theta = 0^\circ$ and $\theta = 90^\circ$ spectra with respect to one another.

III. RESULTS, ANALYSIS, AND DISCUSSION

A. Sb^-

The 351 nm photoelectron spectrum of Sb^- is shown in Fig. 1. The spectrum corresponds to transitions from the negative-ion ground state to various electronic states of the neutral atom, which are assigned in Table I according to well-known⁴ energy levels of the neutral. No evidence of hot bands resulting from electronic excitation of the anion was observed. From the electron binding energy of the ground-ground state transition (transition a in Fig. 1), the

TABLE I. Assignment of the 351 nm photoelectron spectrum of Sb^- including angular distributions.^a

Label	Assignment	eKE (eV)	eBE (eV)	β
a	$4S_{3/2} - 3P_2$	2.485	1.046	0.52
b	$2D_{3/2} - 3P_2$	1.430	2.101	-0.38
c	$2D_{5/2} - 3P_2$	1.263	2.268	-0.48

^aThe spacings in the Sb^- spectrum, which correspond to accurately known atomic energy levels in Sb, were used to calibrate the relative energy scale of the spectrometer. Therefore, the values in this table should not be construed as a measurement of Sb atomic energies.

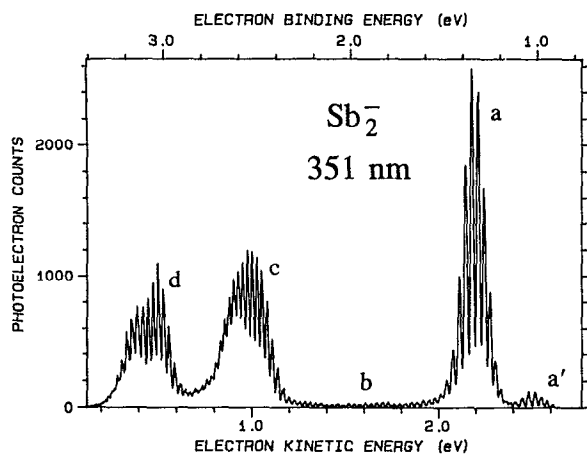


FIG. 2. The 351 nm photoelectron spectrum of Sb_2^- . Three main electronic bands emanating from the Sb_2^- ground state are observed: band a [$^1\Sigma_g^+ \rightarrow ^2\Pi_g(1/2_g)$], band c [$^3\Sigma_u^+ \rightarrow ^2\Pi_g(1/2_g)$], and band d [$^3\Delta_u \rightarrow ^2\Pi_g(1/2_g)$]. In addition an electronic hot band is observed, band a' [$^1\Sigma_g^+ \rightarrow ^2\Pi_g(3/2_g)$], as well as weak transitions (b) to highly vibrationally excited levels of the $^1\Sigma_g^+$ Sb_2 ground state.

electron affinity of Sb is determined to be 1.046 ± 0.005 eV. The measurement is in good agreement with the previously measured⁵ value of 1.07 ± 0.05 eV, but with a tenfold increase in precision.

B. Sb_2^-

1. Results and Franck–Condon analysis

Of the four species examined in the present study, the most extensive new information is obtained for antimony dimer. Figure 2 displays an overview of the 351 nm spectrum, showing three prominent electronic transitions (a, c, and d). Based on the established²³ electronic structure of As_2 and on *ab initio* calculations⁹ of Sb_2 , a, c, and d can be assigned as transitions from the anion ground state [$^2\Pi_g(1/2_g)$] (Ref. 24) to the $^1\Sigma_g^+$, $^3\Sigma_u^+$, and $^3\Delta_u$ states of the neutral. In addition, an electronic hot band is observed (a'), as well as weak continuous vibrational structure (b).

The most unusual feature of the spectrum is the weak continuous vibrational structure that extends almost 1 eV, from the end of band a to the beginning of band c. The peak centers have irregular spacings ranging from 220 to 270 cm^{-1} , and the line shapes are similarly irregular. Although these spacings vary, there is a general tendency toward smaller spacing with increasing electron binding energy, and the highest observed spacing (270 cm^{-1}) is the vibrational frequency observed in band a. Based on these observations we assign feature b to transitions to highly excited vibrational states of the electronic ground state ($^1\Sigma_g^+$) of Sb_2 .

Normally, we expect vibrational transition intensities in photoelectron spectra to be governed by the Franck–Condon principle; however, feature b cannot be explained in these terms. We suggest that the deviation from Franck–Condon intensities is caused by an accidental resonance, where the 351 nm (3.531 eV) light accesses a short-lived state of the negative ion, through which additional levels of

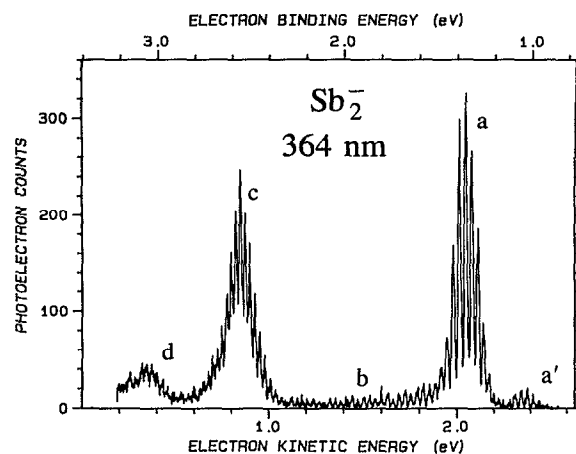


FIG. 3. The 364 nm photoelectron spectrum of Sb_2^- . For ease of comparison, it is plotted on the same electron binding energy scale as Fig. 2. The dramatic changes in intensity profiles between this spectrum and the spectrum in Fig. 2 are due to resonant photodetachment.

the neutral molecule can be accessed. To test this hypothesis we changed the photodetachment wavelength to 364 nm (3.408 eV). Figure 3 displays the 364 nm photoelectron spectrum. Feature b is enhanced, and the intensities and shapes of features c and d have changed completely. For direct photodetachment well above threshold ($> 0.5 \text{ eV}$), a small change in photon energy should merely shift the electron kinetic-energy scale of the spectrum, with very little change in relative intensities. The observed change in intensities is indicative of contributions from resonant photodetachment, and the presence of non-Franck–Condon features at both wavelengths suggests that the excited negative-ion state is very broad. Although the resonance occurs at both wavelengths, the effects are greatly enhanced at 364 nm. Similar behavior has been observed for Cr_2^- ,²⁵ phenoxide ($\text{C}_6\text{H}_5\text{O}^-$),²⁶ S_2^- ,²⁷ and propadienyldiene (C_3H_2^-).²⁷

The irregular spacings and line shapes observed in feature b are most likely due to the intensities of transitions from different negative-ion vibrational states changing relative to one another throughout the progression. The approximate amount of vibrational energy in any neutral state can be determined by the difference in electron binding energy between a given peak and the origin peak in band a. Using our vibrational origin assignment for band a (described subsequently), we count peaks to determine an assignment of $\nu=33$ for the peak at 2.299 eV electron binding energy, with a total vibrational energy (above zero point) of $1.017(6) \text{ eV}$ [$8202(50) \text{ cm}^{-1}$]. The vibrational constants of Gerber and Kuscher⁷ for the ground state of Sb_2 , which include a second-order anharmonicity, predict a vibrational energy of 8222 cm^{-1} above zero point for $\nu=33$. This provides strong support for our assignment of feature b to vibrationally excited states of the Sb_2 electronic ground state.

Interestingly, the only features that are not strongly affected by the change in wavelength are bands a and a'. The simplest explanation for this is that the short-lived

negative-ion state accessed by the resonance is weakly bound (has a large bond length), and autodetaches only to states that sample large internuclear separation. The highest occupied molecular orbitals of Sb_2^- arise from combinations of atomic $5p$ orbitals, resulting in the electronic configuration $\sigma_g^2 \pi_u^4 \pi_g^1$. The transitions of bands a and a' involve detachment from a π_g antibonding orbital to obtain a $^1\Sigma_g^+$ state with a smaller bond length, while bands c and d result from detachment from a π_u bonding orbital resulting in the larger bond length $^3\Sigma_u^+$ and $^3\Delta_u$ states. It appears that the resonant state autodetaches preferentially to the larger bond-length electronic states and to highly vibrationally excited states of the smaller bond-length electronic state—in other words, to vibrational states which sample larger r .

Because the 351 nm spectrum appears to be less affected by the resonance than the 364 nm spectrum, we will use it for the Franck–Condon analysis of bands a', a, c, and d. Since bands a and a' appear to be only slightly affected by the resonance, molecular constants obtained from Franck–Condon simulation of these bands should be reliable. We will also show that bands c and d in the 351 nm spectrum can be modeled as Franck–Condon progressions, each involving transitions to two spin–orbit components of a neutral electronic state, and yielding reasonable molecular constants. However, it is very likely that the profiles of bands c and d are severely affected by the resonance. Therefore, the Franck–Condon simulations of these bands should be viewed only as plausible models of the observed intensities, rather than being definitive.

One concern in the analysis is that the photoelectron spectra were obtained using a mixture of naturally occurring isotopes. Antimony has two naturally occurring isotopes; ^{121}Sb (57.3%) and ^{123}Sb (42.7%). The ensuing Franck–Condon analysis was performed using the reduced mass for the ^{121}Sb – ^{123}Sb isotopomer. Contributions to the spectrum from the other isotopomers are not expected to affect the derived constants within the experimental precision. One might expect the high v' end of a vibrational progression to be slightly broadened by the presence of three isotopomers. However, even at $v'=6$ of the Sb_2 ground state the range of vibrational energies is only 11 cm^{-1} (1.4 meV), which, given the instrumental resolution of 8–10 meV, cannot be distinguished from the broadening caused by vibrational congestion due to hot bands [see Fig. 4(a)].

The Franck–Condon analysis procedure has been described in some detail.²⁰ The anion and neutral electronic states are modeled as Morse oscillators, and Franck–Condon factors are determined by numerical integration of the overlap of the Morse oscillator wave functions. The parameters which can be adjusted in the analysis are the bond-length change, anion and neutral vibrational frequencies and anharmonicities, position and intensity of the origin transition, a Gaussian instrumental linewidth function, and the anion vibrational temperature. The fitting procedure consists of both visual and least-squares optimization of the simulated spectrum to the experimental data. In this manner, the frequency and intensity information

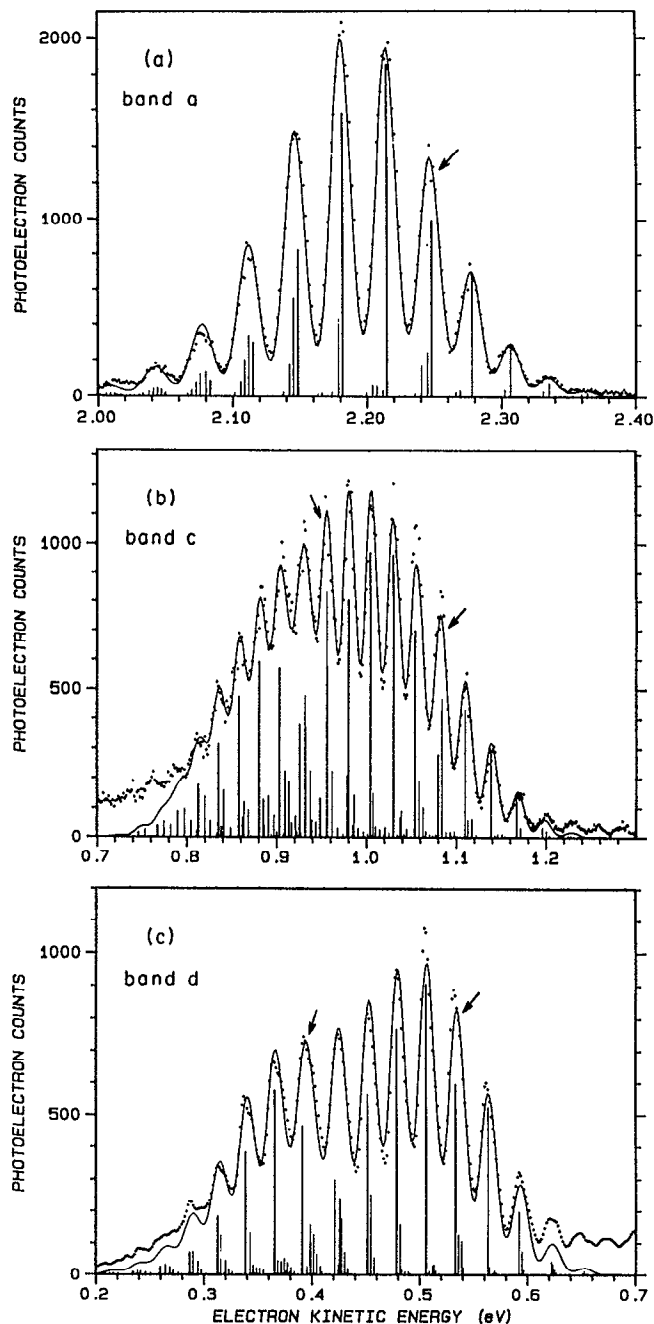


FIG. 4. Franck–Condon simulations of the Sb_2^- electronic bands using the molecular constants in Table II. Data are represented by points, the simulated spectra are drawn as solid lines, and individual vibrational transitions are plotted as sticks. Thick sticks represent transitions from $v''=0$; the remaining structure is due to vibrational hot bands. Arrows indicate vibrationless origins.

contained in the spectrum are simultaneously used to extract molecular constants. Error bars are determined empirically by varying parameters until the quality of the fit degrades significantly (as determined visually); care is taken to ensure that the degradation cannot be offset by adjusting other parameters. Because of the small rotational constant of Sb_2 , the rotational contribution to the line shape is calculated to be less than 1 meV and can be neglected.

TABLE II. Results of Franck–Condon analysis of the 351 nm photoelectron spectrum of Sb_2^- . These are the values used to produce the simulations shown in Fig. 3. The error bars given do not take into account possible deviation from Franck–Condon behavior due to an autodetaching resonance.

State	Bands involving this state ^a	T_0 (cm^{-1}) ^b	T_0 (cm^{-1}) ^c	ω_e (cm^{-1})	$\omega_e X_e^d$ (cm^{-1})	r_e (\AA)
Sb_2^-						
$^2\Pi_g(1/2_g)$	a,b,c,d	0	-10 340 (60)	242 (10)	(1.2)	2.573(10)
$^2\Pi_g(3/2_g)$	a'	2460 (40)		236 (10)	(0.66)	2.571(10)
Sb_2						
$X^1\Sigma_g^+(0_g^+)$	a',a,b		0	269.25 ^e	0.53 ^e	2.4878 ^e
$^3\Sigma_u^+(1_u)$	c		9 420 (60)	205 (10)	(0.95)	2.694(20)
$^3\Sigma_u^+(0_u^-)$	c		10 480 (60)	187 (10)	(0.44)	2.701(20)
$^3\Delta_u(2_u)$	d		13 830 (80)	221 (10)	(0.5)	2.665(20)
$A^3\Delta_u(1_u)$	d		14 970 (80) ^f	215 (10)	(0.5)	2.654(20)

^aBands in photoelectron spectrum (see Fig. 2) in which these states appear as a lower state (anion states) or an upper state (neutral states).

^bReferenced to the Sb_2^- ground state.

^cReferenced to the Sb_2 ground state.

^dAnharmonicity is not well determined in the fit to the spectrum; the values in parentheses were used to obtain the optimized simulations shown in the figures.

^eFixed at value from Ref. 7.

^fOrigin assignment based entirely on term energy from Ref. 8.

Band a was assigned as a transition from the anion ground state [$^2\Pi_g(1/2_g)$] to the neutral ground state [$^1\Sigma_g^+(0_g^+)$], based on its having the lowest binding energy of the three strong bands, and on its vibrational spacing of $270(10) \text{ cm}^{-1}$ being in agreement with previous measurements⁷ of the ground vibrational frequency of Sb_2 . The Franck–Condon analysis of this band was carried out by fixing the neutral state constants at literature values,⁷ and allowing the anion constants and vibrational temperature to vary. To determine the position of the vibrationless origin, several assignments were attempted; only one assignment yielded a suitable fit. The resulting vibrational temperature was $420(50) \text{ K}$, consistent with previous values measured from our ion source. The adiabatic electron affinity was determined to be $1.282 \pm 0.008 \text{ eV}$, the binding energy of the origin peak, labeled with an arrow in Fig. 4(a). The finding that the bond length decreased in going from the anion to the neutral arose from the fit; attempts to simulate the spectrum with a bond-length increase were unsuccessful. The anion constants resulting from the analysis are shown in Table II; the simulated spectrum is illustrated in Fig. 4(a). Table II also contains all of the constants obtained from the Franck–Condon fits described below.

Band a' was fit assuming the electronic hot-band assignment, $^1\Sigma_g^+(0_g^+) \leftarrow ^2\Pi_g(3/2_g)$. The neutral constants were fixed at the values from high-resolution spectroscopy,⁷ and the anion constants were allowed to vary. Based on the vibrational temperature determined in the previous fit, only one origin choice was feasible.

The fit of band a using the accurately known ground-state neutral constants provided the key to the remainder of the analysis. For the fits of bands c and d, the anion molecular constants and vibrational temperature could be fixed. Bands c and d presented additional difficulty because

of the presence of multiple spin–orbit components with overlapping vibrational progressions. Band c is assigned to the $^3\Sigma_u^+$ state with 0_u^- and 1_u components, and band d is assigned to the $^3\Delta_u$ state which has 1_u , 2_u , and 3_u components.

The simulation of band c is shown in Fig. 4(b). First, the high electron kinetic-energy tail of the spectrum was fit as one electronic band; only one vibrational origin was possible given the vibrational temperature of 420 K . The simulation of that electronic band over the entire region was then subtracted from the spectrum, leaving one electronic band behind which could be treated in a similar manner. The two fits were summed and simultaneously fit for all of the data. This procedure was repeated for many combinations of origin assignments; only the assignment shown in Fig. 4(b) yielded a satisfactory fit.

To fit band d, we used molecular constants for the $^3\Delta_u(1_u)$ state which have been determined previously.⁸ Using our Sb_2 electron affinity of 1.282 eV in combination with the $^3\Delta_u(1_u)$ term energy of $14\,991 \text{ cm}^{-1}$, the origin for this state was determined to lie at an electron binding energy of 3.141 eV ($e\text{KE}=0.391 \text{ eV}$ at 351 nm). This origin location was used along with the known neutral state vibrational frequency and an estimated bond length to generate a simulation which could then be subtracted. Although we expected the remaining spectrum to result from transitions to two spin–orbit components of the neutral, it could be simulated as a single electronic transition. An origin was easily assigned, given the fixed vibrational temperature (420 K), and by assuming that the geometry of the neutral state was similar (within 0.02 \AA) to that of the 1_u state. For the final simulations [Fig. 4(c)] the two electronic bands were simultaneously fitted, and the neutral state constants for both electronic bands were allowed to vary.

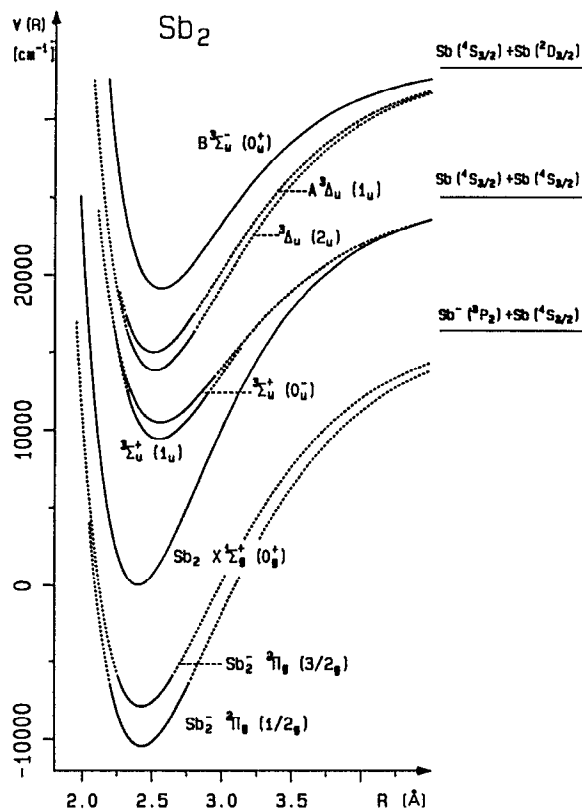


FIG. 5. Approximate potential-energy curves for the low-lying electronic states of Sb_2 and Sb_2^- . Most of the molecular constants used to generate these curves have been determined in the present study (see Table III).

2. Low-lying electronic structure of Sb_2 and Sb_2^-

Approximate potential-energy curves for the Sb_2 and Sb_2^- states observed in this work and the $B^3\Sigma_u^-(0_u^+)$ state⁷ of Sb_2 are shown in Fig. 5. Table III shows molecular constants for these states, obtained from this work, previous experiments, and predicted by *ab initio* methods. Because the photoelectron transitions to the two excited states of Sb_2 are affected by a resonance, those values which rely on intensity measurements (origin assignments and geometry displacements) may not be accurate. Therefore, the term energies and bond lengths obtained for these bands should be regarded as approximate; however, the vibrational frequencies for these states are determined from line spacings and should be reliable.

The vibrational frequencies, spin-orbit splitting, and geometries determined for Sb_2^- are the first experimental determinations of any molecular constant of this anion. The lowered vibrational frequency and increased bond length observed for the anion (compared to the neutral) are consistent with the additional electron residing in an antibonding orbital. The spin-orbit splitting of this $^2\Pi$ state (2460 cm^{-1}) is similar to that of the $^2\Pi$ ground state of SbO (2272 cm^{-1}),²⁸ indicating that it is a typical value for an antimony centered unpaired electron. Our ordering of the $^2\Pi$ spin-orbit components is simply based on Hund's rules.

Most of the Sb_2 neutral states accessed in the photo-

TABLE III. Low-lying electronic states of Sb_2 and Sb_2^- . All units are in cm^{-1} unless otherwise noted.

State	Constant	This work	Previous experiment	<i>ab initio</i> ^a
Sb_2^-				
$^2\Pi_g(1/2_g)$	T_e^b	0		
	ω_e	242 (10)		
	r_e	2.573 (10) Å		
$^2\Pi_g(3/2_g)$	T_e^b	2460 (40)		
	ω_e	236 (10)		
	r_e	2.571 (10)		
Sb_2				
$X^1\Sigma_g^+(0_g^+)$	T_e^c	0	0	0
	ω_e	270 (10)	269.25(10) ^e	259
	r_e		2.4878(45) Å ^c	2.58 Å
$^3\Sigma_u^+(1_u)$	T_e^c	≈9450		8760
	ω_e	205 (10)		199
	r_e	≈2.694 Å		2.78 Å
$^3\Sigma_u^+(0_u^-)$	T_e^c	≈10 520		8847
	ω_e	187 (10)		198
	r_e	≈2.701 Å		2.79 Å
$^3\Delta_u(2_u)$	T_e^c	≈13 855		15 284
	ω_e	221 (10)		199
	r_e	≈2.665 Å		2.77 Å
$A^3\Delta_u(1_u)$	T_e^c	≈15 000 ^d	14 991.5 ^f	15 636
	ω_e	215 (10)	217.0 (4) ^f	198
	r_e	≈2.654 Å		2.77 Å
$^3\Delta_u(3_u)$	T_e^c			15 660
	ω_e			200
	r_e			2.77 Å
$B^3\Sigma_u^-(0_u^+)$	T_e^c		19 067.5 (6) ^e	22 176
	ω_e		217.29 (20) ^e	205
	r_e		2.6587 Å ^c	2.76 Å

^aAll values from Ref. 9.

^bReferenced to the Sb_2^- ground electronic state potential.

^cReferenced to the Sb_2 ground electronic state potential.

^dOrigin assignment based entirely on Ref. 8 term energy.

^eFrom Ref. 7 (^{121}Sb - ^{123}Sb).

^fFrom Ref. 8.

electron spectrum have not been examined previously. For the X and A states, the vibrational frequencies measured in the spectrum are in excellent agreement with the previous experiments. Our analysis employed Gerber and Kuscher's⁷ rovibrational constants for the X state. Gerber and Kuscher demonstrate that the value of $r_{v=2}$ reported by Sfeila *et al.*²⁹ ($r_{v=2} = 2.3415\text{ Å}$) is in error by -0.15 Å . In a recent review,⁶ Balasubramanian compared his *ab initio* r_e value to the $r_{v=2}$ value of Sfeila *et al.* and found a 0.25 Å difference between theory and experiment; the comparison of the *ab initio* value to the accurate Gerber and Kuscher value of r_e is much better (Table III). Our analysis also employed Almy and Schultz's⁸ measurement of the A - X band of Sb_2 at $14\,991\text{ cm}^{-1}$, which was later assigned to the $^3\Delta_u(1_u)$ state by Balasubramanian and Li.⁹ The photoelectron spectrum further confirms this assignment as follows. Based on the ordering of states in both As_2

and Bi_2 and on *ab initio* calculations of Sb_2 , we expect the order of the first three electronic states of Sb_2 to be $^1\Sigma_g^+$, $^3\Sigma_u^+$, and $^3\Delta_u$. Because the $14\,991\text{ cm}^{-1}$ term energy lies within band d, the second excited electronic state we observe, it is assigned to $^3\Delta_u$, and optical selection rules require that it correspond to the 1_u component.

The ordering we use for the Ω components of the $^3\Sigma_u^+$ and $^3\Delta_u$ states is based on the ordering in the *ab initio* calculations.⁹ The transition to the $^3\Delta_u$ state can be accounted for as a transition to only two states, where the additional state is lower in energy than the 1_u state and is assigned as 2_u . A likely explanation for the absence of the 3_u transition, suggested by *ab initio* calculations⁹ (see Table III), is that the splitting between the 1_u and 3_u states is very small and not resolved here.

Balasubramanian and Li⁹ have carried out extensive calculations on the electronic structure of Sb_2 , calculating energies, vibrational frequencies, and bond lengths for 33 electronic states. All of the states observed in this spectrum have been treated at the CASSCF-MRSDCI-RCI [complete-active-space self-consistent-field, multireference singles and doubles configuration-interaction (CI), relativistic CI] level and the results are shown in Table III. The calculations underestimate the term energies of the $^3\Sigma_u^+$ state and overestimate the $^3\Delta_u$ energies by roughly 5%–15%. The biggest discrepancy lies in the splittings between Ω components. Our $^3\Sigma_u^+$ (1_u and 0_u^-) splittings are a factor of 12 larger than those calculated and our $^3\Delta_u$ (1_u and 2_u) splittings are more than a factor of 3 larger. One should recall that our measurements of these splittings may not be entirely reliable due to effects of the resonance on relative intensities. For the $^3\Sigma_u^+$ transition, it is possible that one or both of the vibrational progressions are extended by the resonance resulting in an apparently large splitting. However, for the $^3\Delta_u$ state, previous experiments fix the origin for the 1_u state. We observe transitions to a state much lower in energy than the 1_u state, so we know that this state must exist and that the splittings are greatly underestimated by the calculations. The calculations perform superbly in determining the bond-length changes as a function of the electronic state, although the absolute bond length is consistently about 0.1 \AA too large. The vibrational frequencies are only about $10\text{--}20\text{ cm}^{-1}$ too low.

To summarize, Table III presents the current state of knowledge concerning the lowest 2 eV of the electronic structure of Sb_2 , much of which has been determined in the present study. The first molecular constants determined for Sb_2^- are presented as well.

C. Sb_3^- and Sb_4^- photoelectron spectra

Figures 6 and 7 illustrate the 351 nm photoelectron spectra of Sb_3^- and Sb_4^- . The features labeled in these spectra are catalogued in Table IV. Both spectra contain broad electronic transitions which are not vibrationally resolved. In both cases, state-of-the-art *ab initio* calculations were essential to the interpretation of the observed electronic structure. In addition, the Jahn–Teller effect plays an important role in the electronic structure of both the D_{3h}

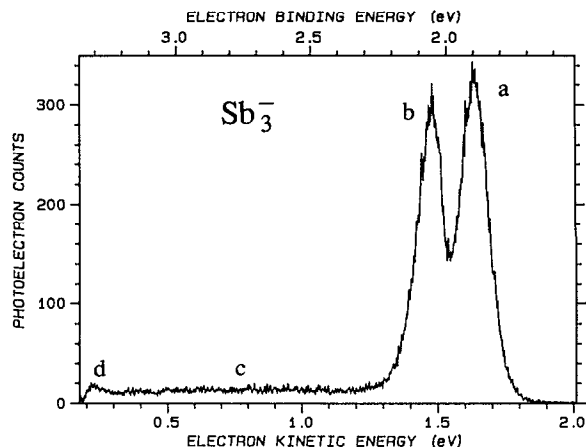


FIG. 6. The 351 nm photoelectron spectrum of Sb_3^- . Three distinct neutral electronic states are observed (features a, b, and d), which are consistent with *ab initio* calculations (Ref. 12) of the electronic structure of equilateral triangular Sb_3 . From feature a, the adiabatic electron affinity of Sb_3 is estimated to be $1.85(3)\text{ eV}$.

trimer and the tetrahedral tetramer. Unlike the previously studied bismuth clusters,² where spin–orbit coupling should quench Jahn–Teller distortion, both effects will contribute to the electronic structure of the lower Z antimony clusters. Unfortunately, the data obtained in this experiment are insufficient to differentiate between these two effects. The lack of vibrational resolution in both spectra prohibits accurate determination of adiabatic electron affinities, although they can be estimated. However, the vertical detachment energies of the anions—the energy required to remove an electron with no geometry change—are determined unequivocally from the peak maxima.

With the exception of N_3 , which is known³⁰ to be linear, the lowest-energy structures of the group V trimers are predicted¹² by *ab initio* theory to be of equilateral triangular geometry, with Jahn–Teller distorted degenerate ground electronic states. Calculations of the negative-ion

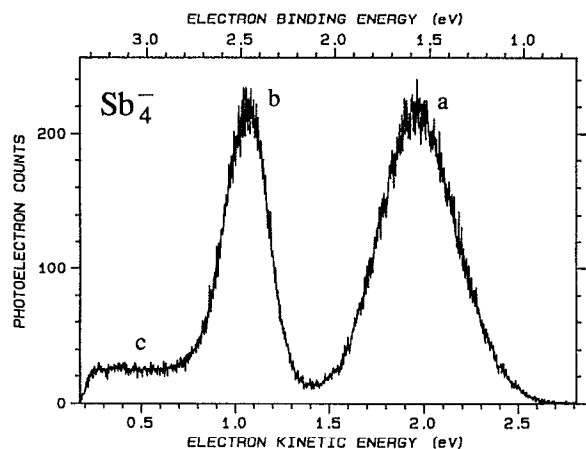


FIG. 7. The 351 nm photoelectron spectrum of Sb_4^- . Two neutral electronic states are observed (features a and b), and the width of feature a suggests that we can only determine an upper bound on the adiabatic electron affinity, $\text{EA}(\text{Sb}_4) < 1.00(10)\text{ eV}$.

TABLE IV. Features in the 351 nm Sb_3^- and Sb_4^- photoelectron spectra. Peak centers and widths are determined by fits to Gaussian line shapes.

Label	Assignment	eKE (eV)	Peak width (FWHM, eV)	β	Comments
Sb_3^-					
a	${}^2A_2(C_{2v}) \leftarrow {}^3A_2'(D_{3h})$	1.628	0.131	-0.53	peak
b	${}^2B_1(C_{2v}) \leftarrow {}^3A_2'(D_{3h})$	1.471	0.127	-0.67	peak
c		0.25-1.35		0.0	continuous, structureless feature
d	${}^2A_2(D_{3h}) \leftarrow {}^3A_2'(D_{3h})$	≈ 0.22			peak
Sb_4^-					
a	${}^1A_1-{}^3T_1$	1.962	0.480	0.29	peak
b	${}^3T_2-{}^3T_1$	1.058	0.288	-0.15	peak
c		0.2-0.8		0.0	continuous, structureless feature

equilibrium structures are more ambiguous. In a high-level treatment of P_3^- , Hamilton and Schaefer³¹ could not conclusively determine whether the lowest-energy structure is triangular or linear. Preliminary calculations of Bi_3^- structures by Balasubramanian³² are similarly ambiguous. Because photodetachment is a vertical, Franck-Condon process, the structure of the negative ion determines which structures of the neutral can be accessed. In our photoelectron spectrum² of Bi_3^- , the agreement of the observed electronic structure with quantum-chemical predictions for the triangular neutral strongly suggested that the spectrum was of triangular, as opposed to linear, Bi_3^- . We reach a similar conclusion for the Sb_3^- spectrum, as is explained below.

The Sb_3^- spectrum contains three peaks and a structureless broad continuum, c. The intensity of peak d, which appears at very low eKE, is severely diminished due to instrumental limitations at electron kinetic energies below 0.3 eV. The three peaks can be readily assigned based on the CASSCF-MRSDCI calculations of Balasubramanian, Sumathi, and Dai¹² on neutral Sb_3 , which predict an equilateral triangular geometry that undergoes Jahn-Teller distortion in degenerate electronic states. Peaks a and b are assigned as transitions from the ground state of Sb_3^- to the ${}^2E''$ ground state of Sb_3 , which is Jahn-Teller distorted into 2A_2 and 2B_2 components. Balasubramanian, Sumathi, and Dai predict a splitting between these components of 0.04 eV, while we measure a splitting of 0.16 eV. The calculations may underestimate the splitting because spin-orbit effects were not included. The observed band contours indicate that similar magnitude geometry changes are involved in each transition. In the case of Jahn-Teller distortion, we might expect roughly equal but opposite geometry changes away from a negative-ion equilateral triangular geometry. Peak d is assigned as a transition from the negative-ion ground state to the first excited state (${}^4A_2''$) of the neutral. This state is predicted to lie 1.31 eV above the ground state; we measure an excitation energy of 1.4 eV.

The negative-ion ground state is assigned in Table IV as ${}^3A_2'$, based both on double occupation of the e'' highest occupied molecular orbital (HOMO) predicted by theory¹² for Sb_3 and on Hund's rules.

From the binding energy of the center of peak a, we determine a vertical detachment energy of 1.90(2) eV. The adiabatic electron affinity of Sb_3 is estimated by assuming that the origin will be shifted from the center of peak a by the same fraction of the linewidth as the similarly shaped and comparably wide band a in the Sb_2^- spectrum, where vibrational resolution permitted rigorous assignment of an origin. The result is an adiabatic electron affinity of 1.85(3) eV.

The photoelectron spectrum of Sb_4^- contains two broad peaks, separated by 0.90 eV. Calculations by Zhang and Balasubramanian¹⁵ at the CASSCF-MRSDCI level predict a T_d geometry for Sb_4 , with a 1A_1 ground state. The HOMO is of e symmetry and the lowest unoccupied molecular orbital (LUMO) is of t_1 symmetry, suggesting a 2T_1 negative-ion ground state. This state will undergo Jahn-Teller distortion, and the absence of electronic hot bands in the photoelectron spectrum indicates that only one component is significantly populated. This seems reasonable, since the photoelectron spectrum of Sb_4 taken by Wang *et al.*¹⁷ probes the 2T_2 excited state of Sb_4^+ and indicates that splittings between components can be on the order of 0.4 eV.

Band a is assigned as a transition from the lowest-energy component of the 2T_1 anion ground state to the 1A_1 ground state of Sb_4 . The broad contour of band a is indicative of the large geometry change associated with the Jahn-Teller distortion, and the band is of similar width to those of Wang *et al.*¹⁷ which were assigned to transitions from the 1A_1 ground state of Sb_4 to components of the 2T_1 excited state of Sb_4^+ . For a T state, distortion can occur along both the $\nu_2(e)$ and $\nu_3(t_2)$ coordinates; the lack of vibrational resolution in band a prohibits determination of the nature of the distortion.

From the peak center of band a, we determine a vertical detachment energy of 1.57(5) eV. The broadness of band a causes difficulties in the determination of an adiabatic electron affinity. The geometry changes involved are likely to be so large that the vibrationless origin is not visible. Wang *et al.*¹⁷ observed bands of similar width (also vibrationally unresolved) in transitions from the 1A_1 ground state of Sb_4 to the 2E ground state of Sb_4^+ . Their models of these bands led to an estimate of the adiabatic ionization potential (IP) at approximately 1.2 eV below the vertical IP. The Sb_4^- spectrum does not contain sufficient information for analogous modeling, since the Jahn–Teller splittings of the anion 2T_1 state are not determined and lack of vibrational resolution precludes determination of the relative roles of the two symmetry-allowed normal coordinates in the distortion. We report the lowest photoelectron energies detectable above the inherent noise level as an upper bound for the electron affinity, $\text{EA}(\text{Sb}_4) < 1.00(10)$ eV.

In light of these findings for the EA of Sb_4 , we suggest a new interpretation of our previously reported² photoelectron spectrum of Bi_4^- . The photoelectron onset for Bi_4^- , which was previously assumed² to correspond to the electron affinity, should rather be regarded as an *upper* bound, resulting in $\text{EA}(\text{Bi}_4) < 1.05(10)$ eV.

Band b can be assigned as a transition to the lowest-energy component of the 3T_2 excited state of the neutral. Zhang and Balasubramanian¹⁵ calculate the state (with undistorted T_d geometry) to be the lowest excited electronic state of Sb_4 , at 2.57 eV above the ground state. We observe a vertical detachment energy to this state that is 0.9 eV above that to the ground state. Because band b is narrower than band a, the band center of band b lies closer to its vibrationless origin than the band center of band a, and the difference in vertical energies of 0.9 eV will be lower than the term energy of the excited state. If we estimate the origin of band b to lie at an eKE of 1.2 eV, and assume that the origin of band a is shifted by a maximum of 1.2 eV from the intensity maximum, we obtain an excitation energy in the range 1.3–2.0 eV, significantly lower than the calculated value of 2.57 eV. As is suggested by Zhang and Balasubramanian, the low excitation energy of this state compared to the calculation is probably due to Jahn–Teller stabilization. The narrowness of band b compared to a is indicative of the similarity of the geometries of the lowest components of the 2T_1 anion and 3T_2 neutral states. Since the transition of band b results from the removal of an electron from a bonding e orbital we expect and observe substantial geometry change; however, it appears that both states are distorted away from the T_d geometry in a similar fashion.

In both the Sb_3^- and Sb_4^- spectra we observe a broad continuous feature, labeled c, which we cannot adequately explain. A similar feature was observed² in the photoelectron spectrum of Bi_3^- . Laser fluence tests showed that the Sb_3^- and Sb_4^- features were due to a one-photon process. One possibility is that we are accessing highly vibrationally excited states of geometries that differ from the equilibrium D_{3h} and T_d structures of the trimer and tetramer. Calculations have not been performed on the stabilities of electronic states that differ from these symmetric structures.

TABLE V. Photoelectron angular distributions for Sb_2^- .

Band	eKE in the 351 nm spectrum (eV)	Range of β in the 351 nm spectrum ^a	Range of β in the 364 nm spectrum
d	0.3–0.6	–0.3 → –0.7	+0.1 → –0.1
c	0.9–1.15	0.0 → –0.55	+0.1 → –0.1
a	2.0–2.3	+0.3 → –0.2	+0.7 → –0.2

^aHigher β values tend to be toward the lower eKE side of each band (see Fig. 8).

lations have not been performed on the stabilities of electronic states that differ from these symmetric structures.

D. Photoelectron angular distributions

The anisotropy parameters for photoelectron angular distributions in the 351 nm spectra of Sb^- , Sb_3^- , and Sb_4^- are listed in Tables I and IV. They are measured with an accuracy of approximately ± 0.1 . For each of these spectra, the anisotropy parameters of the peaks increase with increasing electron kinetic energy. In the eKE region of these spectra this is typical behavior for atomic p electron detachment,³³ and is similar to the behavior seen² for Bi^- and Bi_2^- .

On the other hand, the Sb_2^- angular distributions are very unusual. In the case of direct, nonresonant electron detachment, the anisotropy parameter does not vary significantly over a single electronic transition. For the 351 and 364 nm Sb_2^- photoelectron spectra, the presence of a resonance causes large changes in angular distributions through the progressions. Table V shows the range of anisotropy parameters observed for different vibrational peaks in bands a, c, and d in both the 351 and 364 nm spectra. For feature b, the signal was too weak for accurate determination of the anisotropy parameter. For the 351 nm

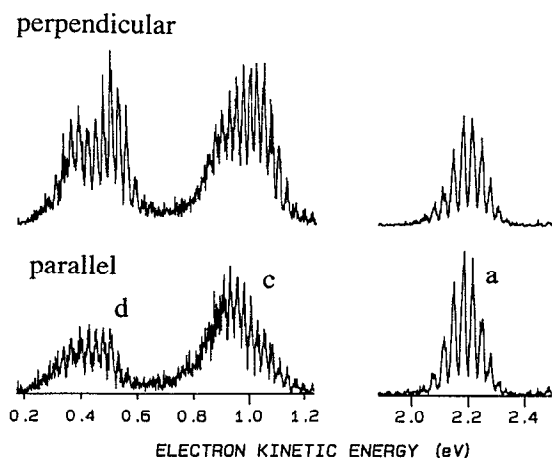


FIG. 8. Bands a, c, and d of the 351 nm photoelectron spectrum of Sb_2^- taken at laser polarizations parallel and perpendicular to the electron ejection direction. The intensities of the parallel and perpendicular spectra are plotted on the same intensity scale; however, the intensities of band a are not to scale with respect to those of bands c and d. The change in band profiles between the two laser polarizations illustrates the variation in anisotropy parameter across a single band (see Table V), and is a signature of resonant photodetachment.

TABLE VI. Electron affinities (eV) of group V atoms, dimers, trimers, and tetramers.

Element	Atom	Dimer	Trimer	Tetramer
N	$<0^a$	$<0^b$	2.68(1) ^c	
P	0.7465(3) ^a	0.589(25) ^d		
As	0.81(3) ^a	0.70(10) ^e		
Sb	1.046(5) ^f	1.282(8) ^f	1.85(3) ^f	$<1.00(10)^f$
Bi	0.946(10) ^a	1.271(8) ^g	1.60(3) ^g	$<1.05(10)^h$

^aReference 35.^bReference 36.^cReference 39.^dReference 37.^eOur interpretation of data in Feldmann *et al.* (Ref. 38).^fThis work.^gReference 2.^hReinterpretation of the value in Ref. 2 as an upper bound.

spectrum, the spectrum in which the effects of the resonance are weaker, the p -like trend of increasing β with increasing eKE of each band is preserved despite the resonance, and can be seen in Table V. However, the anisotropy parameters for individual vibrational peaks show a general trend of decreasing β with increasing eKE within each band. Figure 8 shows normalized 351 nm spectra of bands a, c, and d taken at both parallel and perpendicular polarizations. The dramatic changes in band profiles are indicative of the large changes in β . The 364 nm spectrum, where the resonance effects are stronger, no longer exhibits the expected trend of increasing β with increasing eKE. Instead, we observe virtually isotropic angular distributions for bands c and d. Band a, which is least affected by the resonance, displays the same trend as for the 351 nm spectrum, where β tends to decrease with increasing eKE within the band, although the range of values is considerably larger.

Similar variations in β across electronic transitions and with photodetachment wavelength have been observed in the photoelectron spectrum of carbon monoxide³⁴ and in our own²⁷ photoelectron spectrum of S_2^- ; in both of these cases the effects can be attributed to autoionizing or autodetaching resonances. Although the short-lived resonances account for these variations qualitatively, a detailed theoretical understanding of the autoionizing state is necessary in order to account for the observed angular distributions. At present, this problem is theoretically intractable for a heavy-atom molecule such as Sb_2^- . The continuous features in the Sb_3^- and Sb_4^- spectra, labeled c, could not be assigned and are not understood. Within experimental uncertainty, the photoelectron angular distributions for these features are isotropic.

E. Electron affinity trends and thermochemistry

Table VI summarizes the electron affinities^{2,35–39} of small group V atoms and clusters. Some important trends are evident. First, the electron affinities of Sb_{1-4} and Bi_{1-4} not only follow the same pattern, but are very similar in magnitude. The relatively high electron affinities of the trimers are not surprising, because all of the other neutral species have special stabilities associated with their elec-

tronic configurations. The group V atoms have a half-filled p shell (s^2p^3 configuration), the dimers are closed shell in their ground state (“triple-bonded” $\sigma^2\pi^4$ configuration), and the tetramers have a closed-shell 1A_1 configuration. The trimer, on the other hand, has a singly occupied e'' orbital, and addition of an electron leads to a half-filled orbital.

One surprising measurement is that the electron affinities of the Sb and Bi dimers are greater than those of the atoms. The electron affinity difference between the atom and dimer corresponds to the difference in anion and neutral dissociation energy via

$$D_0(X_2^-) - D_0(X_2) = \text{EA}(X_2^-) - \text{EA}(X^-). \quad (2)$$

The electron affinities in Table VI show that for As_2 and P_2 the dissociation energy decreases upon addition of an electron, the anticipated result for addition into an antibonding orbital. On the other hand, the dissociation energies of Bi_2 and Sb_2 increase upon electron addition, although the changes in equilibrium properties (bond length and vibrational frequency) behave in accord with addition into an antibonding orbital. From Eq. (2) and the Sb_2 dissociation energy [$D_0^0(\text{Sb}_2) = 71.2 \pm 1.0$ kcal/mol (3.09 ± 0.04 eV)] determined from mass-spectrometric measurements of high-temperature equilibria,¹⁸ we determine an Sb_2^- dissociation energy, $D_0(\text{Sb}_2^-)$, of 76.8 ± 1.0 kcal/mol (3.33 ± 0.04 eV).

IV. CONCLUSIONS

We have reported the 351 nm laser photoelectron spectra of small antimony cluster anions, obtaining the electron affinities (Table VI) of antimony atom, dimer, and trimer, and an upper bound for the electron affinity of antimony tetramer. The electron affinities of the antimony clusters are very similar to those recently reported for the small clusters of bismuth, another group V metal. All of the spectra display electronic structure, which is vibrationally resolved only for the dimer. The observed electronic structure can be explained in terms of high-level *ab initio* calculations by Balasubramanian and co-workers^{9,12,15}

The Sb_2^- spectrum displays unusual intensities and photoelectron angular distributions which indicate that photodetachment is mediated by an autodetaching resonance that is accessed at the photodetachment wavelength (351 nm). These unusual effects are enhanced when the wavelength is changed to 364 nm. This study and other recent negative-ion photoelectron spectra show that the possibility of an accidental resonance must always be a consideration in the interpretation of a photoelectron spectrum.

Note added in proof. In Ref. 2, the ground electronic state of D_{3h} bismuth trimer mentioned throughout Secs. III C and III E should be $^2E''$, not $^2E'$. The resulting spin-orbit components in the D_{3h} double group are then $E_{1/2}$ and $E_{3/2}$, not $E_{3/2}$ and $E_{5/2}$. The authors thank Dr. J. Berkowitz and Professor K. Balasubramanian for calling attention to this error.

ACKNOWLEDGMENTS

The authors thank K. Balasubramanian for providing results before publication. Support was provided by the National Science Foundation, Grants No. CHE88-19444 and No. PHY90-12244.

- ¹For example, *Metal Clusters*, edited by M. Moskovits (Wiley-Interscience, New York, 1986), and references therein.
- ²M. L. Polak, J. Ho, G. Gerber, and W. C. Lineberger, *J. Chem. Phys.* **95**, 3053 (1991).
- ³J. Ho, M. L. Polak, and W. C. Lineberger, *J. Chem. Phys.* **96**, 144 (1992).
- ⁴C. E. Moore, *Atomic Energy Levels*, Natl. Bur. Stand. (U.S.) Circ. 467 (U.S. GPO, Washington, DC, 1952).
- ⁵D. Feldmann, R. Rackwitz, E. Heinicke, and H. J. Kaiser, *Z. Phys. A* **282**, 143 (1977).
- ⁶K. Balasubramanian, *Chem. Rev.* **90**, 93 (1990).
- ⁷The most precise constants for the *X* and *B* states of Sb_2 are in G. Gerber and G. Kuscher, *Chem. Phys.* **60**, 119 (1981).
- ⁸G. M. Almy and H. A. Schultz, *Phys. Rev.* **51**, 62 (1937).
- ⁹K. Balasubramanian and J. Li, *J. Mol. Spectrosc.* **135**, 169 (1989).
- ¹⁰H. Sontag and R. Weber, *Chem. Phys.* **70**, 23 (1982).
- ¹¹B. Eberle, H. Sontag, and R. Weber, *Surf. Sci.* **156**, 751 (1985).
- ¹²K. Balasubramanian, K. Sumathi, and D. Dai, *J. Chem. Phys.* **95**, 3494 (1991).
- ¹³J. Drowart and P. Goldfinger, *J. Chim. Phys.* **55**, 721 (1958).
- ¹⁴V. E. Bondybey, G. P. Schwartz, and J. E. Griffiths, *J. Mol. Spectrosc.* **89**, 328 (1981).
- ¹⁵H. Zhang and K. Balasubramanian, *J. Chem. Phys.* (submitted).
- ¹⁶L. S. Wang, Y. T. Lee, D. A. Shirley, K. Balasubramanian, and P. Feng, *J. Chem. Phys.* **93**, 6310 (1990).
- ¹⁷L. S. Wang, B. Niu, Y. T. Lee, D. A. Shirley, E. Ghelichkhani, and E. R. Grant, *J. Chem. Phys.* **93**, 6318 (1990); **93**, 6327 (1990).
- ¹⁸J. Kordis and K. A. Gingerich, *J. Chem. Phys.* **58**, 5141 (1973).
- ¹⁹J. Ho, K. M. Ervin, and W. C. Lineberger, *J. Chem. Phys.* **93**, 6987 (1990).
- ²⁰K. M. Ervin and W. C. Lineberger, in *Advances in Gas Phase Ion Chemistry*, edited by N. G. Adams and L. M. Babcock (JAI, Green-

wich, CN, in press), Vol. 1.

- ²¹D. M. Neumark, K. R. Lykke, T. Andersen, and W. C. Lineberger, *Phys. Rev. A* **32**, 1890 (1985).
- ²²J. Cooper and R. N. Zare, *J. Chem. Phys.* **48**, 942 (1968).
- ²³L. A. Heimbrook, N. Chestnoy, M. Rasanen, G. P. Schwartz, and V. E. Bondybey, *J. Chem. Phys.* **83**, 6901 (1985).
- ²⁴Electronic state assignments are given in Hund's case a (case c) notation, i.e., $^{2S+1}\Lambda_p(\Omega_p)$, where *p* designates parity (gerade or ungerade).
- ²⁵S. M. Casey, P. W. Villalta, A. A. Bengali, C.-I. Cheng, J. P. Dick, P. T. Fenn, and D. G. Leopold, *J. Am. Chem. Soc.* **113**, 6688 (1991).
- ²⁶R. F. Gunion, M. K. Gilles, M. L. Polak, and W. C. Lineberger, *Int. J. Mass Spectrom. Ion Proc.* **117**, 601 (1992).
- ²⁷M. L. Polak and W. C. Lineberger (unpublished).
- ²⁸K. P. Huber and G. Herzberg, *Constants of Diatomic Molecules* (Van Nostrand Reinhold, New York, 1979).
- ²⁹J. Sfeila, P. Perdigon, F. Martin, and B. Femelat, *J. Mol. Spectrosc.* **42**, 239 (1972).
- ³⁰A. E. Douglas and W. J. Jones, *Can. J. Phys.* **43**, 2216 (1965).
- ³¹T. P. Hamilton and H. F. Schaefer III, *Chem. Phys. Lett.* **166**, 303 (1990).
- ³²K. Balasubramanian (private communication).
- ³³D. Hanstorp, C. Bengtsson, and D. J. Larson, *Phys. Rev. A* **40**, 670 (1989).
- ³⁴B. Wannberg, D. Nordfors, K. L. Tan, L. Karlsson, and L. Mattsson, *J. Electron Spectrosc.* **47**, 147 (1988).
- ³⁵H. Hotop and W. C. Lineberger, *J. Phys. Chem. Ref. Data* **14**, 731 (1985).
- ³⁶G. J. Schulz, *Rev. Mod. Phys.* **45**, 423 (1973).
- ³⁷J. T. Snodgrass, J. V. Coe, C. B. Freidhoff, K. M. McHugh, and K. H. Bowen, *Chem. Phys. Lett.* **122**, 352 (1985).
- ³⁸D. Feldmann, R. Rackwitz, H. J. Kaiser, and E. Heinicke, *Z. Naturforsch. A* **32**, 600 (1977). The value we quote for the electron affinity of As_2 is based on our own interpretation of the photodetachment threshold data in this publication, where we assume that the thresholds are at the electron affinities. Similar interpretation of the thresholds for P_2 and S_2 data in the same publication leads to electron affinities that are within ± 0.05 eV of the more accurate values later measured by laser photoelectron spectroscopy.
- ³⁹R. E. Continetti, D. R. Cyr, R. B. Metz, and D. M. Neumark, *Chem. Phys. Lett.* **182**, 406 (1991).